Journal of Catalysis 323 (2015) 10–18

Contents lists available at ScienceDirect

Journal of Catalysis

journal homepage: www.elsevier.com/locate/jcat

The functionalisation of graphite surfaces with nitric acid: Identification of functional groups and their effects on gold deposition

Rebecca Burgess [a], Carlo Buono [a], Philip R. Davies [a,*], Robert J. Davies [b], Thomas Legge [a], Amy Lai [a], Ryan Lewis [a], David J. Morgan [a], Neil Robinson [a], David J. Willock [a]

[a] Cardiff Catalysis Institute, School of Chemistry, Cardiff University, Cardiff CF10 3AT, United Kingdom
[b] Imperial College, London SW7 2AZ, United Kingdom[1]

ARTICLE INFO

Article history:
Received 8 November 2014
Revised 17 December 2014
Accepted 18 December 2014

Keywords:
Gold
Carbon
Graphite
Catalysis
AFM
XPS
Hydroxyl groups
Nucleation

ABSTRACT

The role of surface oxygen species in the nucleation and reactions of metal nanoparticles on carbon surfaces has been explored using model systems based on graphite supported with DFT calculations. Features in the X-ray photoelectron spectra at characteristic binding energies of 532.6 eV, 531.8 eV, and 533.5 eV were unambiguously assigned to hydroxyl, ketone, and ether groups after selective derivatization. Surfaces treated with nitric acid generate almost exclusively hydroxide groups which on heating to 573 K transform into ketones and ethers. Gold nanoparticles deposited from an aurochloric acid solution show a better dispersion on the hydroxylated surface than on either the clean or the ketone-covered surface and whereas on the hydroxylated surface the adsorbed gold was reduced completely to Au^0, a small component attributed to Au^{3+} was present after deposition at the ketone-/ether-covered surface. DFT calculations confirm that gold atoms adsorb more strongly to a hydroxylated step edge than one functionalised with ketone groups. The results give an insight into the effects of the acid washing of carbon catalysts before loading with the active metal components.

1. Introduction

Carbon surfaces are ubiquitous in heterogeneous catalysis with distinct advantages of weight, cost, and the ease with which functional materials supported by carbons can be recovered. Over the last fifty years it has become established practice that the carbons used in this way are treated with acids before the adsorption of the active component, the removal of contaminants being cited as the main justification for this step. However, recent work by Hutchings et al. at Cardiff, has demonstrated that the acid wash has a much more significant role than simply removing contaminants affecting both selectivity and activity of the resulting catalytic materials. An example is the direct synthesis of hydrogen peroxide where washing the carbon support in nitric acid gave a sixfold improvement in selectivity over washing the carbon in hydrochloric acid without significantly impacting the activity [1,2].

The complex surface chemistries associated with different carbons present a considerable challenge when it comes to unravelling the processes involved in reactions over the surface and in understanding how the carbons interact with the active materials they support. A great deal of research has been done studying metal deposition on graphite surfaces (Highly Ordered Pyrolytic Graphite, "HOPG") under vacuum where surface functionality is removed [3]. However, this ignores the role that surface functionality might play in the nucleation, stability, and chemistry of metal nanoparticles on carbon surfaces.

Our approach to this complex area has been to focus on surfaces that are as reproducible as possible and HOPG is an ideal starting point being readily available in well characterised orientations and quality. The experimental protocol we have adopted mimics that of the preparation of supported gold catalysts for the hydrochlorination of ethyne and we hope eventually to explain the effects that acid washing has on the performance of these and other catalysts [2,4,5]. In an initial investigation [6], we explored changes in the topography of HOPG surfaces after treatment with water and dilute acids under ambient conditions. Atomic force microscopic imaging revealed the presence of 50–100 nm wide topographical features "bubbles" approximately 4–10 nm in height depending on acid strength. These were attributed to local areas of delamination which DFT calculations suggest are probably associated with existing defects that have been functionalised with oxygen-containing groups; we speculate that these groups somehow reduce the interlayer bonding.

* Corresponding author. Fax: +44 29 2087 4030.
E-mail address: daviespr@cardiff.ac.uk (P.R. Davies).
[1] Present address.

http://dx.doi.org/10.1016/j.jcat.2014.12.021
0021-9517/

The importance of the functional groups at carbon surfaces is well known. Goncalves et al. [7] for example, demonstrated the involvement of the oxygen functionality in the attachment of gold nanoparticles to graphene but were unable to distinguish between the roles of the different possible oxygen groups. Temperature-programmed desorption (TPD) and infrared spectroscopy (IR) have commonly been used for this purpose but the former is rather indirect and IR is only reliable for the identification of functional groups with strong transition dipoles. The difficulty of unambiguously identifying functional groups at carbon surfaces has been highlighted in reviews by Boehm [8] and Rodríguez-reinoso [9].

X-ray photoelectron spectroscopy (XPS) is a surface sensitive and quantitative tool that has great potential in this area [10–12] but there remains uncertainty about species assignments in XPS because of the huge complexity of the materials involved. Everhart and Reilley [13] and Batich [14] have described an XPS method that highlights particular functional groups over the others present. The method involves selective chemical derivatization of specific functional groups and has been applied to the study of the functionality of polymer and carbon nanotube surfaces [15–17].

In a recent paper [18], we have used the selective derivatization method to establish that treatment of HOPG surfaces with HCl generates almost exclusively hydroxyl groups and that subsequent heating (to 573 K) converts all of the hydroxyl groups to a mixture of ketone and ether functionalities. The AFM images show that this also removes all of the acid induced "bubbles". Deposition of gold onto these surfaces was also examined briefly but the data were limited to relatively high gold coverages. In the present paper, we explore whether the chemistry is similar on nitric acid-treated HOPG surfaces and study the deposition onto these surfaces of more catalytically relevant coverages of gold nanoparticles from aqueous solution.

2. Experimental

HOPG samples (~10 mm square, ZYH quality, supplied by NT-MDT ltd, Europe) were cleaned before each experiment by peeling off the top few graphene monolayers using adhesive tape. Acid treatment involved placing a 100 μl droplet of fresh 0.5 M HNO_3 (Fischer Chemicals Ltd, 99%) and leaving to stand for 30 min before drying under a pure helium stream. The acid wet the surface very effectively, and so larger droplets were not needed to provide complete coverage of the crystal surfaces. Gold deposition was achieved in a similar fashion: 100 μl droplet of a gold precursor solution (2×10^{-6} M, $HAuCl_4 \times H_2O$, Sigma–Aldrich, 99.999%), was placed on the pre-treated sample and left for 1 min. The sample was subsequently dried under a stream of helium for 2 min.

Ultra-pure water ("UPW", Millipore) was used for dilution of the acids before surface treatment and also for control experiments that replicated dosing and analysis conditions. Selected samples were heated to 423 K and 573 K for 1 h after surface treatment and allowed to cool to ambient temperature before analysis.

Derivatization reagents: trifluoroacetic anhydride (TFAA, 99%), trifluoroethyl hydrazine (TFH, 70 wt% in water), trifluoroethanol (TFE, 99%), and N-N′-di-tert-butylcarbodiimide (DTBC, 99%) were purchased from Sigma–Aldrich and used as received. Derivatization reactions were carried out in a sealed glass chamber pumped with a rotary vane pump to a base pressure of $\sim 10^{-2}$ mbar. (Initial attempts at derivatization using a stainless steel vacuum chamber were abandoned because subsequent analysis by XPS showed transport of copper from the metal vacuum seals to the HOPG surfaces. No contamination issues occurred in the glass chamber.) 2 ml of TFAA and TFH liquids were frozen and placed into a reservoir of liquid nitrogen inside the chamber; this enabled the evacuation of the chamber without pumping away the reactant. TFE on the other hand was dosed from a 2 ml mixture of TFE, pyridine, and DTBC in a 9:4:8 ratio respectively, according to the recipe reported by Everhart and Reilley [13]. HOPG samples were placed into the chamber avoiding contact with the reservoir and walls. The chamber was evacuated until the liquid nitrogen reservoir had evaporated at which point it was isolated from the pump and allowed to equilibrate for ~24 h. The chamber was opened to air and the samples typically were analysed by XPS within a few hours of removal. However, control experiments in which the derivatised samples were allowed to stand in air for up to 7 days showed no significant change in the surface chemistry.

Repeated experiments have shown that the concentration of different oxygen components in the XP spectra of the treated HOPG surfaces was slightly variable from sample to sample (±20%); quantitative estimates between samples are therefore difficult. However, binding energies of the components within the spectra were highly reproducible from sample to sample.

XP spectra were recorded with a Kratos Axis Ultra-DLD photoelectron spectrometer using a monochromatic Al Kα X-ray source and the "hybrid spectroscopy" mode resulting in an analysis area of 700 × 300 μm at a pass energy of 40 eV for high resolution scans and 160 eV for survey scans. The XPS data were analysed using CasaXPS [19] with all binding energies referenced to the C(1s) peak at 284.5 eV and have an uncertainty of ~0.2 eV. Curve fits were made using Gaussian line profiles and surface concentrations were calculated using the method described in detail by Carley et al. [20,21]. AFM images were acquired on a Bruker Veeco Multimode probe in tapping mode using silicon nitride tips. AFM images were analysed using WSxM software [22].

To support the experimental investigation, spin-polarised density functional theory (DFT) calculations were performed within the periodic plane-wave basis set code VASP 5.3 [23–26]. Projector augmented waves (PAW) potentials have been used to describe the ion cores leaving valence electronic configurations $C(2s^2 2p^2)$, $O(2s^2 2p^4)$, and $Au(6s^1 5d^{10})$ to be explicitly calculated whilst the ultrasoft pseudopotential has been employed for the H atoms. Exchange–correlation interaction was treated by generalised gradient approximation (GGA) in the parameterisation of Perdew, Burke, and Ernzerhof (PBE). The weak van der Waals interactions operating between the graphitic layers have been taken into account by the semi-empirical method of Grimme, DFT-D2 [27], as implemented in VASP. The dispersion coefficient, C_6, and van der Waals radius, R_0, for gold were taken to be 40.62 J nm^6 mol^{-1} and 1.772 Å, respectively, as reported by Amft et al. [28]. For calculations on the bulk unit cell a k-point mesh of 5 × 5 × 3 was used which was reduced for the supercell calculations on surfaces to 3 × 3 × 1, in either case a Monkhorst–Pack grid was used for k-point sampling [29,30]. The plane-wave basis set was defined by a 500 eV cutoff for all calculations. The width of the Gaussian smearing for the occupation of electronic levels was 0.01 eV and for surface calculations dipole corrections along the three directions of the unit cell vectors were included. All structures were optimised until a convergence of 10^{-5} eV was reached and the Hellman–Feynman forces on each relaxed ion were smaller than 10^{-4} eV Å^{-1}. In calculations on surfaces all atoms in the cell are optimised with the cell size and shape held fixed.

The hexagonal unit cell of the most common Bernal structure for graphite [30–33] has experimental lattice constants of $a_0 = b_0 = 2.46$ Å and $c_0 = 6.78$ Å with $\gamma = 120°$ [32,33]. Following the above methodology these unit cell dimensions were optimised by a systematic scaling of the a_0 and b_0 lattice parameters, which define the intra-layer periodicity, followed by scaling of the c_0 parameter, which gives the inter-layer repeat distance. The optimised cell parameters are $a_0 = b_0 = 2.465$ Å and $c_0 = 6.297$ Å. The in-plane C—C bond length of 1.420 Å is in good agreement with

the experimental value of 1.421 Å [33,34]. The inter-layer separation 3.149 Å is shorter than observed experimentally (3.354 Å) [34,35] by ~6% although it is in line with previous simulations using similar functionals [35,36].

Functionalisation of graphite is expected to take place preferentially at step edges where the more reactive edges of graphene sheets are available. Graphene simulation of the functionalization of sheet edges with oxygen-containing groups has been studied in detail by Mauri and co-workers [34,36–38]. We have chosen to work with stable termination at armchair edges which present isolated C=C bonds for addition of oxygen species. The unit cell was first redefined as $a = a_0$, $b = a_0 + 2b_0$, $c = c_0$, in this setting armchair step edges are created for Miller indices (10X) with X controlling the terrace length. All the simulations were performed using the (1 0 5) surface which gave sufficient separation between step edges for Au to be adsorbed at an effectively isolated step edge. The thickness of the simulation cell was set so that four aromatic rings separate oxygen functionalities on the same graphene sheet but opposite sides of the slab. We also employ a 2×2 surface supercell for all slab calculations so that periodic images of Au atoms are well separated in the direction parallel to the step edge and there are three empty steps in the simulations cell (Fig. 9). This gives a slab which contains 144 C, 16 O, and 32 H atoms.

The adsorption energies of a gold atom at functionalised surfaces have been calculated by the expression

$$E_{ads} = E_{(Surf.+Gold\ atom)} - E_{(Surf.)} - E_{(Gold\ atom)}$$

where $E_{(Surf.)}$ is the energy of the surface, $E_{(Gold\,atom)}$ represents the energy of the adsorbate in gas phase. A negative adsorption energy indicates exothermicity and favourable adsorption.

3. Results and discussion

3.1. XPS and AFM studies of acid-treated HOPG

AFM imaging shows that HOPG surfaces treated with 0.5 M HNO_3 under ambient conditions become decorated with raised approximately circular features 50–100 nm in diameter and ~15–20 nm in height above the surrounding lattice, Fig. 1. We have previously demonstrated that these features are due to local areas of delamination, possibly due to the functionalization of defected sites and the reduction in interlayer bonding and shown that the size of the islands is related to acid concentration [6]. Control experiments using ultra-pure water in contrast, showed neither the local delamination effects nor any significant change in the species present at the surface.

The corresponding XP spectra are shown in Fig. 2 and reveal a single peak in the O(1s) region at 532.8 eV with a calculated surface concentration of 6.3×10^{14} cm^{-2} corresponding to ~0.16 monolayers. Changes in the C(1s) spectrum are too small to be detected against the background carbon signal but there is a small increase in the N(1s) region with the development of a peak with a surface concentration corresponding to ~1.4×10^{14} cm^{-2} at a binding energy of 400.2 eV indicative of an amine rather than a nitrate.

Heating the sample in stages causes a decrease in the *number* of features in the AFM images with an accompanying decline in the overall *volume* of the features. Unlike HCl however, some features still remain after heating to 573 K. In the XP spectra the peak in the N(1s) regions vanishes by 573 K whereas the single peak in the oxygen region splits into two with binding energies of 531.8 and 533.5 eV. There is no significant change in the surface oxygen concentration on heating from 290 K to 573 K.

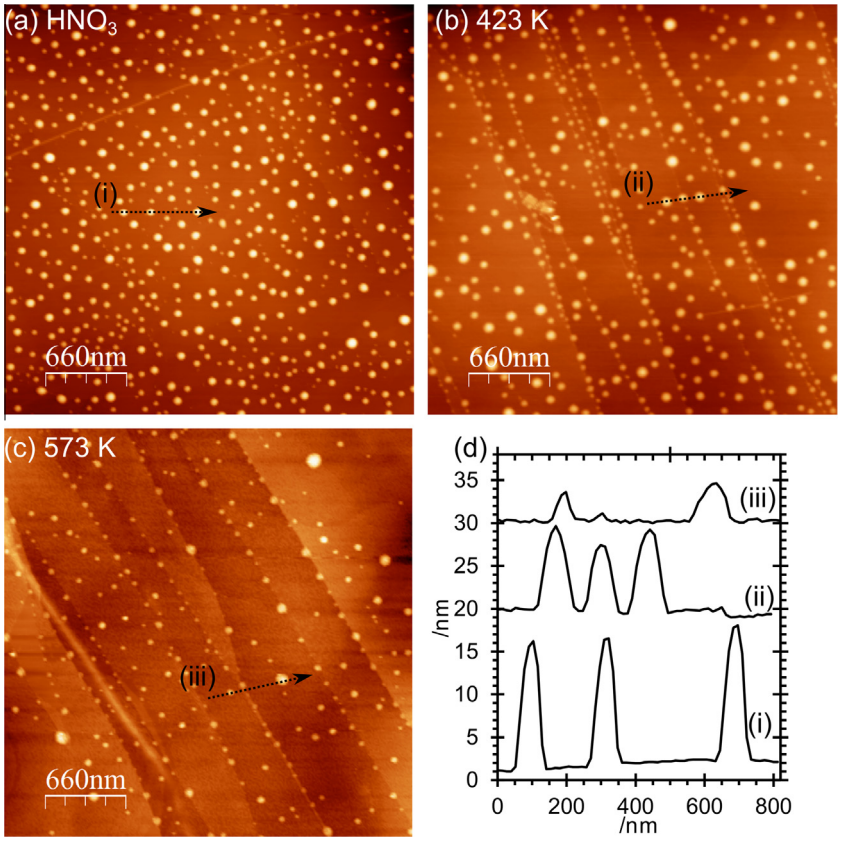

Fig. 1. AFM images of the acid-treated surfaces: (a) HOPG surface treated with 0.5 M HNO_3 for 30 min; (b) after heating to 423 K for 1 h; (c) after heating to 573 K for 1 h; (d) line profiles recorded from the AFM images.

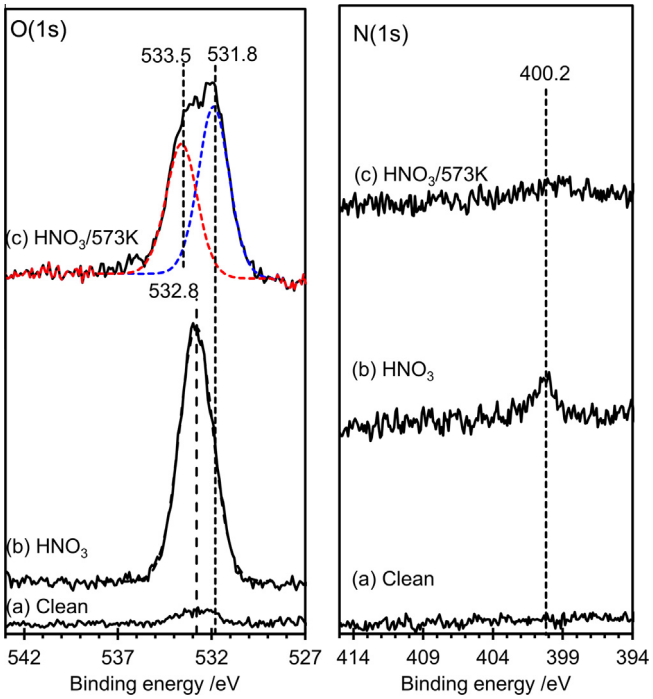

Fig. 2. XP spectra of HOPG after treatment with 0.5 M HNO_3 and subsequent heating to 573 K. (a) Clean surface; (b) after treatment with 0.5 M HNO_3 for 30 min; (c) after heating to 573 K for 1 h and cooling to ambient.

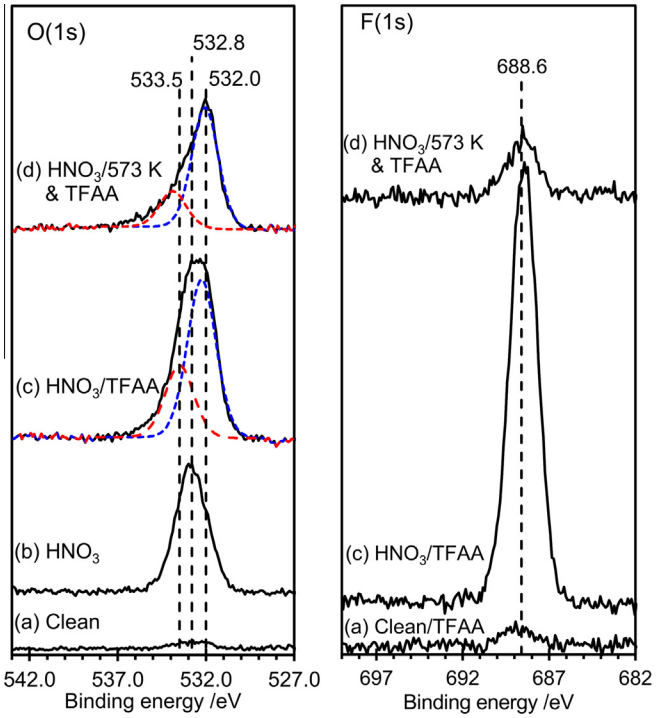

Fig. 3. XP spectra showing O(1s) and F(1s) regions of HOPG after treatment with HNO_3 and TFAA. (a) Clean HOPG exposed to TFAA; (b) (in O(1s) spectra only for comparison), HOPG treated with 0.5 M HNO_3 for 30 min; (c) surface in (b) after exposure to TFAA; (d) after heating (b) to 573 K for 1 h followed by exposure to TFAA.

3.2. Identification of functional groups at acid-treated HOPG surfaces by selective derivatization and XPS characterisation

3.2.1. Identifying hydroxyl groups at carbon surfaces

Trifluoroacetic anhydride (TFAA, $CF_3C(O)OC(O)CF_3$) reacts selectively with hydroxyl groups at carbon surfaces with a 1:1 stoichiometry and high selectivity, generating an adsorbed fluoroacetate and an acetic acid that desorbs or reacts with other hydroxyl groups to give the same product [14,39]

$$CF_3C(O)OC(O)CF_3(g) + OH(a) \rightarrow CF_3C(O)O{-}(a) + CF_3CO_2H(g) \quad (1)$$

HOPG surfaces, freshly cleaved in air, always show a small concentration ($\sim 1 \times 10^{14}\ cm^{-2}$) of oxygen with a maximum in XP peak intensity at ~532.6 eV. Exposure of this surface to TFAA leads to a similarly weak peak in the F(1s) spectrum (Fig 3a); further exposure to TFAA did not give rise to any further adsorption of TFAA (not shown). The HOPG surface after treatment with 0.5 M HNO_3 was exposed to TFAA at room temperature. On reaction with the TFAA, the strong O(1s) peak at 532.8 eV broadened with the development of a shoulder to higher binding energy. Curve-fitting of the spectra shows that the resulting envelope is consistent with peaks at 531.8 eV and 533.5 eV with area ratio of ~3:1. In the F(1s) region a strong peak at 688.6 eV indicates the presence of fluorine with a surface concentration that is a little less than twice that of the oxygen peak at 533.5 eV.

The data suggest that the HNO_3 treatment of graphite surfaces generates a high concentration of hydroxyl species, with a characteristic binding energy of ~532.7 eV. The fluoroacetate produced from the reaction of the TFAA with this hydroxyl will have two distinct oxygen species, a carbonyl and a methoxy type functionality (C—O—CF_3). The former can be assigned unambiguously to the O(1s) peak at 533.5 eV whilst the other must contribute to the peak at 532 eV. The larger intensity of the 532 eV peak compared with the 533.5 peak suggests that some intensity from the original peak before TFAA treatment remains. This implies that either unreacted OH groups remain at the surface after TFAA treatment or a second species is present with a binding energy similar to the OH. Exposure of the *heated* HCl-treated surface to TFAA results in negligible reaction; the small amount of fluorine that is present is probably due to hydroxyl groups formed at the HOPG surface whilst the sample was transferred from the oven to the treatment chamber. The absence of significant amounts of fluorine clearly indicates that heating to 573 K is sufficient to convert all of the surface hydroxyl groups to other functionalities. This confirms the observations from Fig. 2.

3.2.2. Identifying carboxylic acid groups at carbon surfaces

Trifluoroethanol (TFE, CF_3CH_2OH in the presence of DTBC) reacts selectively with carboxylic acid groups at carbon surfaces eliminating water with a 1:1 stoichiometry and high selectivity [13–15]

$$CF_3CH_2OH(g) + {-}CO_2H(a) \rightarrow CF_3C(OH)O{-}(a) + H_2O(g) \quad (2)$$

The clean and treated HOPG surfaces were exposed to the TFE/DTBC mixture for 24 h; the resulting XP spectra are shown in Fig. 4. No reaction was observed between the TFE and the clean HOPG surface and exposure of the heated HNO_3-treated surface to the TFE/DTBC mixture also results in only a minimal uptake in fluorine Fig 4b. The corresponding O(1s) spectra are within 0.1 eV of the spectra observed without TFE treatment. We can conclude that mild HNO_3 treatment of the HOPG surface does not lead to significant quantities of carboxylic functionality. Fig. 4c shows that there is also no reaction between TFE and either of the states generated by heating the acid-treated surface.

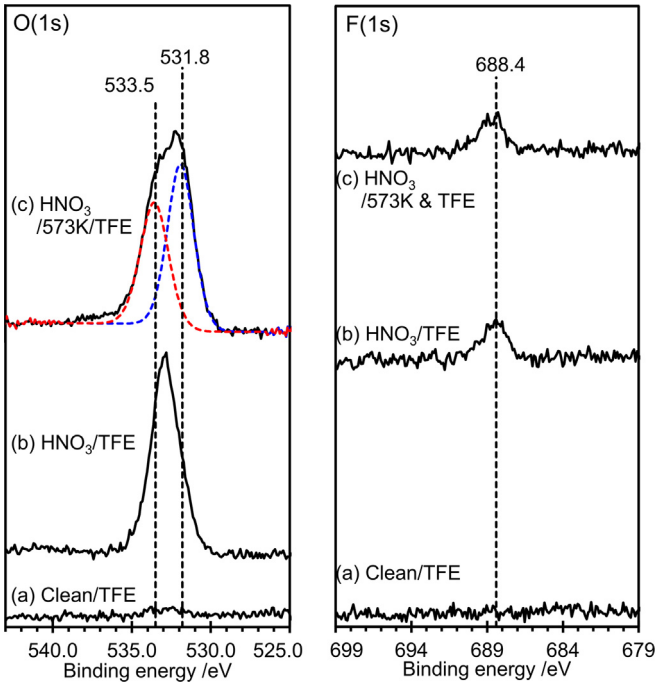

Fig. 4. XP spectra of HNO_3-treated HOPG surface exposed to TFE vapour. (a) Clean HOPG surface exposed to TFE; (b) HOPG surface treated with 0.5 M HNO_3 and subsequently exposed to TFE; (c) HOPG surface treated with 0.5 M HNO_3 and heated for 1 h to 573 K before exposure to TFE.

We can therefore rule out the assignment to carboxylic groups of either of the two species with O(1s) binding energies of 531.8 and 533.5 eV.

3.2.3. Identifying ketone groups at carbon surfaces

Trifluoroethyl hydrazine (TFH, $CF_3CH_2NH{-}NH_2$) reacts selectively with carbonyl groups at carbon surfaces eliminating water with a 1:1 stoichiometry [13–15]

$$CF_3CH_2NH{-}NH_2(g) + {-}CO(a) \rightarrow CF_3CH_2NH{-}N{=}(a) + H_2O(g) \quad (3)$$

Exposure of the clean HOPG to TFH results in no reaction Fig 5a. Exposure of the HNO_3-treated surface to TFH on the other hand does produce a small amount of fluorine at the surface with a corresponding peak in the N(1s) region. This differs from the same experiment [18] using a HCl wash suggesting that the nitric acid does generate some ketone groups at the surface. However, exposure of the HOPG surface to TFH after HNO_3 washing and subsequent heating to 573 K results in much more extensive reaction. A strong peak develops in the fluorine region at 688.4 eV accompanied by a strong peak at 400.5 eV in the N(1s) region. Interestingly, although the reaction stoichiometry (Eq. (3)) indicates complete removal of the oxygen, two oxygen features remain in the XP spectra after TFH treatment. A possible explanation is that the water is not completely desorbed but rather reacts with the lattice in a concerted reaction with the hydrazine reaction; furthermore, a hydroxyl group would be a possible assignment for the peak at 531.9 eV since its close proximity to the hydrazine group could be sufficient to shift the OH binding energy significantly from that of the hydroxyl group observed after HCl treatment.

3.3. Gold deposition at acid-treated and heated HOPG surfaces

The ability to isolate specific oxygen functionalities at the graphite surface allows us to explore how different oxygen species influence gold nucleation from solution on carbon. In Fig. 6, XP spectra are shown from the adsorption of gold on HOPG surfaces containing mostly hydroxyl groups and mostly ketones and ethers.

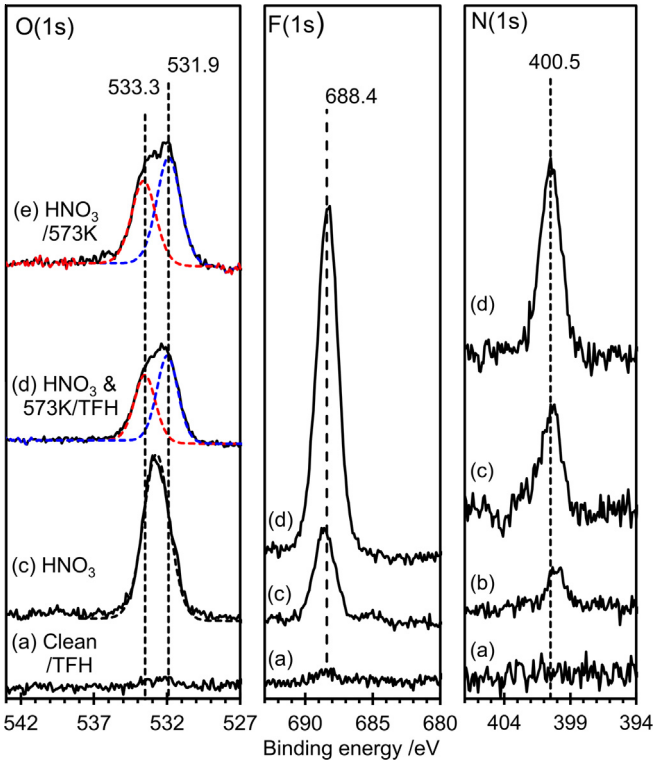

Fig. 5. XP spectra of HNO_3-treated HOPG surface exposed to TFH vapour. (a) Clean HOPG surface exposed to TFH; (b) (N(1s) spectra only), HOPG surface treated with 0.5 M HNO_3; (c) HOPG surface treated with 0.5 M HNO_3 and subsequently exposed to TFH; (d) HOPG surface treated with 0.5 M HNO_3 and heated for 1 h to 573 K before exposure to TFH; (e) (O(1s) spectra only), HNO_3-treated surface heated to 573 K surface *without* TFH exposure for comparison.

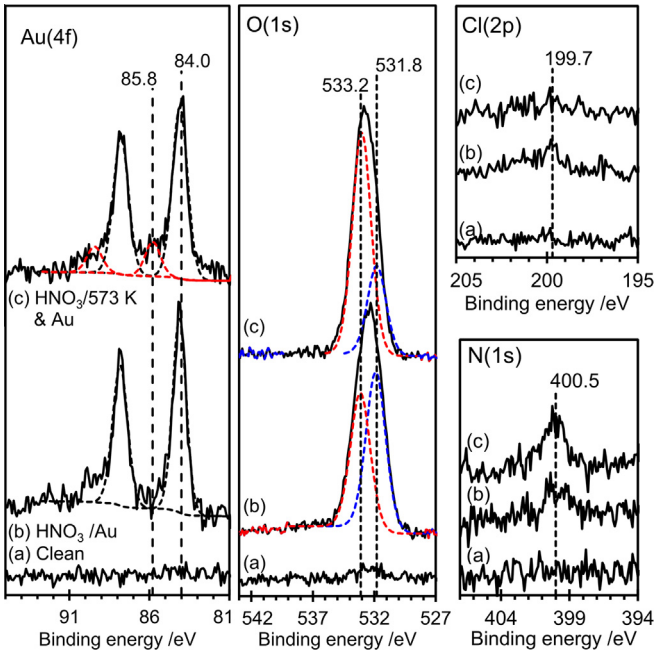

Fig. 6. XP spectra of the HOPG surface after gold deposition from a solution of chloroauric acid: (a) Clean surface; (b) HOPG surface treated with 0.5 M HNO_3, dried and then exposed to a 2×10^{-6} M solution of $HAuCl_4$; (c) HOPG surface treated with 0.5 M HNO_3, dried and heated to 573 K (1 h) before cooling and being exposed to 2×10^{-6} M solution of $HAuCl_4$.

The spectra show a single gold state in the case of the former with a characteristic Au $\left(4f_{\frac{7}{2}}\right)$ peak at 84.0 indicating Au^0. The surface covered with ketones and ethers on the other hand clearly shows a second component at 85.8 eV. Possible assignments of this peak are to a Au^{3+} species or to small nanoparticles of gold which are known to show higher binding energies than the bulk. Under continued exposure to the X-ray beam however, the 85.8 eV peak reduces in intensity, behaviour that is characteristic of a Au^{3+} state that is slowly reducing in the X-ray beam [40]. There is however very little intensity in the Cl(2p) spectra in contrast to the situation with HCl-washed HOPG where higher gold concentrations were used.

3.3.1. Characterisation of gold deposition with Atomic Force Microscopy

Gold deposition on the treated surfaces was studied by AFM Figs. 7 and 8. An earlier study of gold deposition on HCl-treated surfaces used a chloroauric acid concentration of 6×10^{-6} M, but this gave relatively high gold coverages; the present study uses a concentration of 2×10^{-6} M, and this gives results more comparable to those expected on a real catalyst. It is clear from the AFM images that acid treatment has a direct effect on the gold nucleation; on the freshly cleaned HOPG surface, Fig 7a, the majority of gold nucleation is at step edges. In contrast, a much higher dispersion of nanoparticles is obtained on the HNO_3-treated surface, and unlike the clean surface, the nanoparticles are not obviously linked with step edges, many being situated in the middle of terraces. Gold nucleation over the acid-treated surface that has been heated to convert the hydroxyls into ketones and ethers shows many fewer but larger gold particles (30×50 nm) than at the hydroxylated surface. These are again frequently associated step edges.

For comparison, our earlier study of gold deposition on HCl-modified surfaces was repeated with the lower concentration of gold used above for the nitric acid experiments. Very similar behaviour to that at the HNO_3-treated surface was observed with a much better dispersion of smaller particles nucleating at the OH-covered surface whereas the ketone-/ether-covered surface gave a relatively poor dispersion of larger particles. In the present study, we cannot discriminate between the images of gold deposited at the HCl and nitric acid-treated surfaces.

3.4. DFT calculations for Au atoms at oxygen functionalised step edges

Periodic DFT calculations using the PBE + D2 approach were used to give structures for an armchair edge containing hydroxyl and ketone functional groups. In each case, the additional valency of the edge carbon atoms is taken up with H atoms. In our previous work, we considered the energetics of producing the hydroxylated edge from reaction with water and determined the lowest energy arrangement of the functional groups along the step edge [18]. To accommodate adsorption of a gold atom, we have used a cell doubled in the step edge direction for this work. For the ketone functionalised edge, we have moved the hydroxyl H atom to the neighbouring edge carbon atom, so that the slab structures have the same stoichiometry. This gives simple models to compare the adhesion of gold to the two types of surface oxygen-containing groups on the graphite surface. The relaxed structures of the functionalised edges are shown in Fig. 9a and b. In both cases, the oxygen groups move significantly out of the plane of the graphene

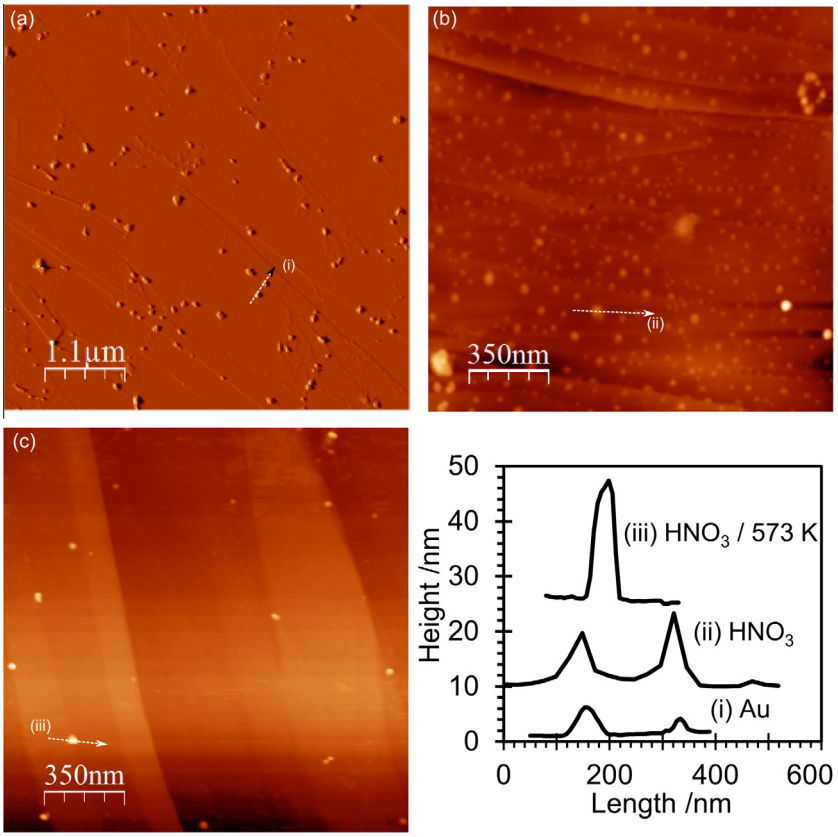

Fig. 7. AFM images of the HOPG surface after gold deposition from a solution of chloroauric acid: (a) Freshly cleaved HOPG surface exposed to a 2×10^{-6} M solution of $HAuCl_4$; (b) HOPG treated with 0.5 M HNO_3, dried and then exposed to a 2×10^{-6} M solution of $HAuCl_4$; (c) HOPG treated with 0.5 M HNO_3, dried and heated to 573 K (1 h) before cooling and exposure to 2×10^{-6} M solution of $HAuCl_4$; (d) line profiles from the AFM images.

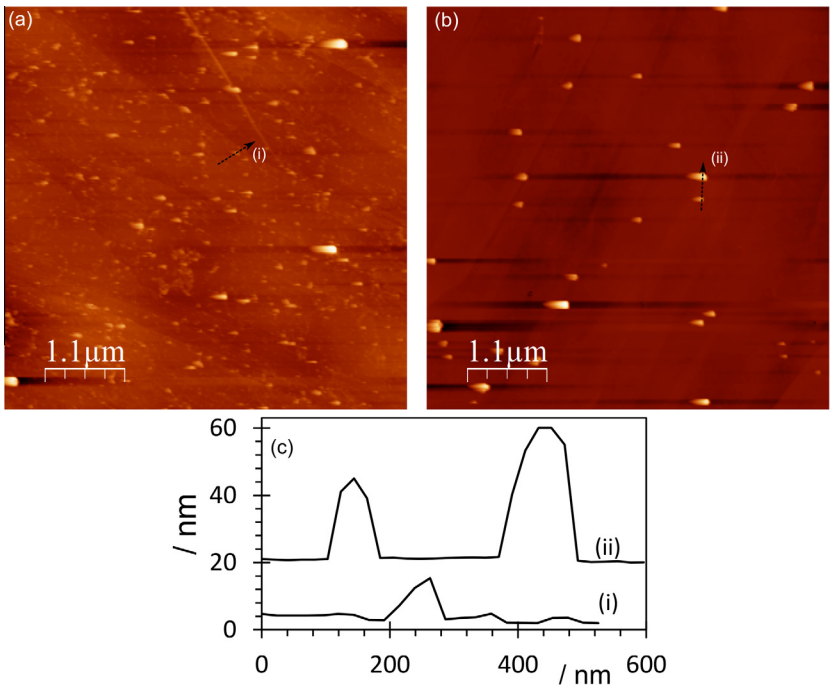

Fig. 8. AFM images of the HOPG surface after gold deposition from a solution of chloroauric acid: (a) HOPG surface treated with 0.5 M HCl, dried and then exposed to a 2×10^{-6} M solution of $HAuCl_4$; (b) HOPG surface treated with 0.5 M HCl, dried and heated to 573 K (1 h) before cooling and being exposed to 2×10^{-6} M solution of $HAuCl_4$; (c) line profiles from the AFM images.

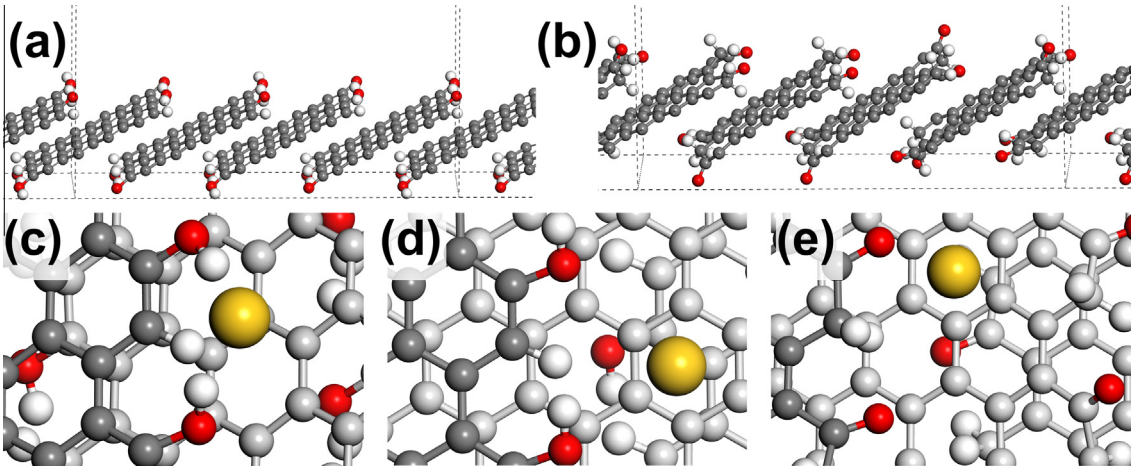

Fig. 9. The slab structure of (a) the hydroxylated step edge and (b) the ketone-containing step edge, dashed black lines show periodic boundaries. Optimised structures of (c) Au at the OH(2) h/C site, (d) Au at the OH(1) h/C site, and (e) Au at the CO h/C site. In all figures, atoms colours are C: grey, H: white, O: red, and Au: yellow. (For interpretation of the references to colour in this figure legend, the reader is referred to the web version of this article.)

sheet and so cause local rumpling of the surface in the immediate region of the edges.

To place a gold atom on the surface, we attempted several initial starting points which differed in location relative to the step edge oxygen functionalization and to the C atoms of the terrace. The layered structure of graphite gives two distinct surface C atoms in the basal (0001) plane of the hexagonal unit cell: (i) a carbon in the top layer can be over another in the second layer, "C/C", or (ii) a carbon atom in the top layer can be over a ring centre in the second layer, "C/h". All surface layer ring centres have a C atom in the second layer below them, "h/C". Table 1 summarises the adsorption energies calculated for a single gold atom. For the hydroxylated step edge, (105) OH, the most stable site identified places the gold atom within 2.1 Å of two hydroxyl groups and over a ring centre of the underlying terrace, OH(2) h/C, as shown in Fig. 9c. This gives an adsorption energy of −1.27 eV which is considerably more favourable than interaction with a single OH group at (105) OH(1), h/C (Fig. 9d). Placing the gold atom further out from the step edge on the section of exposed terrace did not lead to any local minima, rather the gold atom moved back to one of these adsorption sites near to the hydroxyl groups of the step edge. For the ketone-functionalised step edge, we find only sites in which Au is interacting with a single oxygen atom, such as the (105) CO, h/C structure shown in Fig. 9e. This leads to adsorption energies in the range −0.67 to −0.77 eV. These are comparable with the hydroxylated calculations with a single OH interaction, but it appears that the

Table 1
Comparison of calculated properties of Au atom adsorption at O functionalised step edges and the graphite basal plane.

Structure	E_{ads} (eV)	Au···O(H)[d] (Å)	Au···C (Å)
(105) OH(2)[a], h/C[c]	−1.27	2.109, 2.077	4.391
(105) OH(1)[a], h/C[c]	−0.68	2.835, 3.537	3.312
(105) CO[b], h/C[c]	−0.77	2.281	3.187
(105) CO[b], C/h[c]	−0.67	2.402	3.139
(0001) C/C	−0.43	–	2.382
(0001) C/h	−0.44	–	2.356
(0001) h/C	−0.36	–	3.036

Notes:
[a] The hydroxylated edge as shown in Fig. 9a.
[b] The ketone-containing edge as shown in Fig. 9b.
[c] Position of the Au atom relative to the terrace atoms as defined in the main text.
[d] For hydroxylated edge measurements, refer to the closest of the O and H from the OH group.

additional flexibility of the hydroxyl due to rotation around the C—O(H) bonds allows multiple Au···OH interactions and so higher binding energies.

As a further comparison, we also considered Au adsorption to the basal (0001) plane of pure graphite using similar slab models. Here the adsorption energies calculated for Au are around 0.25 eV weaker than any of the step edge adsorption energy values. This indicates that preferential adsorption at oxygen functionalised sites will take place and, coupled with the observation that Au migrates from terrace to step edges on optimisation, suggests that the oxygen functional groups will give nucleation centred for Au particle formation.

4. Conclusions

The XPS data reported here are in complete agreement with that reported for the treatment of graphite with HCl [18]. Both the nitric and hydrochloric acid washing of HOPG surfaces generates almost exclusively surface hydroxyl groups with a characteristic O(1s) binding energy of 532.7 eV. This lies at the lower end of the range of binding energies suggested by Yue et al. [12] and Zielke et al. [11] for hydroxyls on carbon fibres and is slightly lower than that observed for OH groups attached to aliphatic polymers [10]. It is significantly lower than that of hydroxyl groups associated with aromatic polymers even allowing for the difference in reference levels. As in the case of HCl, TFE treatment of the acid-washed surface and the acid-washed/heated surfaces showed no evidence for the presence of any carboxylic functionality. The presence of such groups on carbon surfaces has generally only been reported after treatment with much higher acid concentrations than were used here [41,42]. In future work, we will explore the possibility that the hydroxyl groups are the first stage in the oxidation process and carboxylic acid functionality develops later.

The two oxygen species formed on heating the hydroxyl groups to 573 K have characteristic binding energies of 531.8 and 533.5 eV. The former reacts strongly with TFH and can be assigned to a surface ketone whereas the higher binding energy peak is unaffected by treatment with any of the reagents used in this study. We provisionally assign this state, to an ether-type group (—C—O—C—).

The identification and isolation of the different oxygen functionalities on HOPG allow us to begin to probe the role of particular groups on the adsorption of gold from a chloroauric acid solution. Very low concentrations of gold were necessary to achieve gold coverages relevant to those used in gold catalysis, and at these concentrations, the XPS indicates that the majority of the gold on the surface is reduced to Au^0 although at the ketone-/ether-covered surface a small component attributed to Au^{3+} is also present. The more striking change is the higher dispersion of gold on the acid-treated surface seen in the AFM images. This suggests that adhesion and nucleation of the gold are much better at the OH-covered surface than at the ketone-covered surface. The latter conclusion is supported by the DFT + D2 calculations reported here: whilst the calculations show that the interaction of gold with single hydroxyl or ketone groups leads to similar adsorption energies, the rotational flexibility of the OH group allows for structures in which Au atoms interact with more than one functional groups leading to stronger binding than in the case of the ketone where only one group interacts with the gold atoms. Initial charge density analysis indicates that the main component of the interaction of the Au^0 with the surface is through Au polarisation. Further calculations are underway to investigate the role of the Au oxidation state.

Our results provide an interesting glimpse into the anchoring of metal nanoparticles onto carbon surfaces, with —OH(a) being identified as a more effective surface functional group for encouraging metal dispersion over carbon than —C=O(a). The unambiguous assignment of XP binding energies to particular functional groups and the ability to isolate single types of functional groups at the surface create a useful model system for systematic investigations of functional groups at carbon surfaces.

Acknowledgments

This research was supported by EPSRC Grant EP/I038748/1. TL and RB were supported by the Nuffield Foundation research placement scheme; AL was supported by the Analytical Chemistry Trust Fund summer projects scheme and Cardiff University's CUROP scheme. Via our membership of the UK's HPC Materials Chemistry Consortium, which is funded by EPSRC (EP/L000202), this work made use of the facilities of HECToR and ARCHER, the UK's national high-performance computing service, which is funded by the Office of Science and Technology through EPSRC's High End Computing Programme. Computing resource was also provided by Advanced Research Computing at Cardiff (ARCCA) and the HPC-Wales supercomputer facilities.

References

[1] J.K. Edwards, S.J. Freakley, A.F. Carley, C.J. Kiely, G.J. Hutchings, Acc. Chem. Res. 47 (2014) 845–854.
[2] J.K. Edwards, B. Solsona, E.N. N, A.F. Carley, A.A. Herzing, C.J. Kiely, G.J. Hutchings, Science 323 (2009) 1037–1041.
[3] D. Appy, H. Lei, C.-Z. Wang, M.C. Tringides, D.-J. Liu, J.W. Evans, P.A. Thiel, Prog. Surf. Sci. 89 (2014) 219–238.
[4] M. Conte, A.F. Carley, C. Heirene, D.J. Willock, P. Johnston, A.A. Herzing, C.J. Kiely, G.J. Hutchings, J. Catal. 250 (2007) 231–239.
[5] M. Conte, C.J. Davies, D.J. Morgan, T.E. Davies, D.J. Elias, A.F. Carley, P. Johnston, G.J. Hutchings, J. Catal. 297 (2013) 128–136.
[6] E. Bouleghlimat, P.R. Davies, R.J. Davies, R. Howarth, J. Kulhavy, D.J. Morgan, Carbon 61 (2013) 124–133.
[7] G. Goncalves, P.A.A.P. Marques, C.M. Granadeiro, H.I.S. Nogueira, M.K. Singh, J. Grácio, Chem. Mater. 21 (2009) 4796–4802.
[8] H.P. Boehm, Carbon 40 (2002) 145–149.
[9] F. Rodríguez-reinoso, Carbon 36 (1998) 159–175.
[10] G. Beamson, D. Briggs, High Resolution XPS of Organic Polymers: The Scienta ESCA300 Database, Wiley, Chichester [England]; New York, 1992.
[11] U. Zielke, K.J. Hüttinger, W.P. Hoffman, Carbon 34 (1996) 983–998.
[12] Z.R. Yue, W. Jiang, L. Wang, S.D. Gardner, C.U. Pittman Jr., Carbon 37 (1999) 1785–1796.
[13] D.S. Everhart, C.N. Reilley, Anal. Chem. 53 (1981) 665–676.
[14] C.D. Batich, Appl. Surf. Sci. 32 (1988) 57–73.
[15] A. Chilkoti, B.D. Ratner, D. Briggs, Chem. Mater. 3 (1991) 51–61.
[16] L.A. Langley, D.E. Villanueva, D.H. Fairbrother, Chem. Mater. 18 (2006) 169–178.
[17] K.A. Wepasnick, B.A. Smith, K.E. Schrote, H.K. Wilson, S.R. Diegelmann, D.H. Fairbrother, Carbon 49 (2011) 24–36.
[18] C. Buono, P.R. Davies, R.J. Davies, T. Jones, J. Kulhavy, R. Lewis, D.J. Morgan, N. Robinson, D.J. Willock, Faraday Discuss. 173 (2014) 257–272.
[19] N. Fairley, CasaXPS Manual: 2.3.15 Spectroscopy, Casa Software Ltd, 2009.

[20] A.F. Carley, M.W. Roberts, Proc. R. Soc. London, Math. Phys. Sci. 363 (1978) 403–424.
[21] A.F. Carley, P.R. Davies, R.V. Jones, K.R. Harikumar, G.U. Kulkarni, M.W. Roberts, Surf. Sci. 447 (2000) 39–50.
[22] I. Horcas, R. Fernandez, J. Gomez-Rodriguez, J. Colchero, J. Gomez-Herrero, A. Baro, Rev. Sci. Instrum. 78 (2007) 013705.
[23] G. Kresse, J. Hafner, Phys. Rev. B 47 (1993) 558–561.
[24] G. Kresse, J. Hafner, Phys. Rev. B 49 (1994) 14251–14269.
[25] G. Kresse, J. Furthmuller, Phys. Rev. B 54 (1996) 11169–11186.
[26] G. Kresse, J. Furthmuller, Comput. Mater. Sci. 6 (1996) 15–50.
[27] S. Grimme, J. Comput. Chem. 27 (2006) 1787–1799.
[28] M. Amft, S. Lebegue, O. Eriksson, N.V. Skorodumova, J. Phys.: Condens. Matter 23 (2011) 395001.
[29] H. Monkhorst, J. Pack, Phys. Rev. B 13 (1976) 5188–5192.
[30] R. Haering, Can. J. Phys. 36 (1958) 352–362.
[31] H. Lipson, A.R. Stokes, Proc. R. Soc. London, Ser. Math. Phys. Sci. 181 (1942) 101–105.
[32] D. McKie, C. McKie, Essentials of Crystallography, second ed., Blackwell Science Inc, 1986.
[33] D.R. Lide, CRC Handbook of Chemistry and Physics, 85th ed., CRC Press, 2004.
[34] A.P. Seitsonen, A.M. Saitta, T. Wassmann, M. Lazzeri, F. Mauri, Phys. Rev. B 82 (2010) 115425.
[35] G. Graziano, J. Klimes, F. Fernandez-Alonso, A. Michaelides, J. Phys.: Condens. Matter 24 (2012) 424216.
[36] T. Wassmann, A.P. Seitsonen, A.M. Saitta, M. Lazzeri, F. Mauri, J. Am. Chem. Soc. 132 (2010) 3440–3451.
[37] T. Wassmann, A.P. Seitsonen, A.M. Saitta, M. Lazzeri, F. Mauri, Phys. Status Solidi B: Basic Solid State Phys. 246 (2009) 2586–2591.
[38] T. Wassmann, A.P. Seitsonen, A.M. Saitta, M. Lazzeri, F. Mauri, Phys. Rev. Lett. 101 (2008) 096402.
[39] F. Pippig, S. Sarghini, A. Holländer, S. Paulussen, H. Terryn, Surf. Interface Anal. 41 (2009) 421–429.
[40] Y.-Y. Fong, B.R. Visser, J.R. Gascooke, B.C.C. Cowie, L. Thomsen, G.F. Metha, M.A. Buntine, H.H. Harris, Langmuir 27 (2011) 8099–8104.
[41] I.W. Chiang, B.E. Brinson, R.E. Smalley, J.L. Margrave, R.H. Hauge, J. Phys. Chem. B 105 (2001) 1157–1161.
[42] N. Dementev, X. Feng, E. Borguet, Langmuir 25 (2009) 7573–7577.